**Supporting Information**

# Rapid Dissolution of ZnO Nanoparticles Induced by Biological Buffers Significantly Impacts Cytotoxicity

*Josh E. Eixenberger†‡, Catherine B. Anders†‡, Rebecca J. Hermann†, Raquel J. Brown⊥, Kongara M. Reddy‡, Alex Punnoose‡ and Denise G. Wingett*†*

†Biomolecular Sciences PhD program, ‡Department of Physics, ⊥Biomolecular Research Center, Boise State University, Boise, Idaho 83725, United States

*Corresponding author. Email: denisewingett@boisestate.edu

*Current Address: 1910 W. University Dr., Boise, Idaho 83725. Fax: 208-392-1430. Phone number: 208-426-2921*

**Supporting information content**. UV/vis and spectrofluorometric monitoring of dissolution, Cellular media component screening, X-ray diffraction, FTIR nZnO vs Controls, X-ray photoelectron spectroscopy control, High-resolution TEM images, additional morphological TEM images and description of time-lapsed video

## ABBREVIATIONS

nZnO, zinc oxide nanoparticles; NP, nanoparticles; ROS, reactive oxygen species; XRD, X-ray powder diffraction; XPS, X-ray photoelectron spectroscopy; ICP-MS, inductively coupled plasma mass spectrometry; TEM, transmission electron microscopy; MOPS, 3-Morpholinopropane-1-sulfonic acid; PIPES, 1,4-Piperazinediethanesulfonic acid; TES, 2-[[1,3-dihydroxy-2-(hydroxymethyl)propan-2-yl]amino]ethanesulfonic acid; BES, N,N-Bis-(2-hydroxyethyl)-2-aminoethanesulfonic acid; Tricine, N-(2-Hydroxy-1,1-bis(hydroxymethyl)ethyl)glycine;

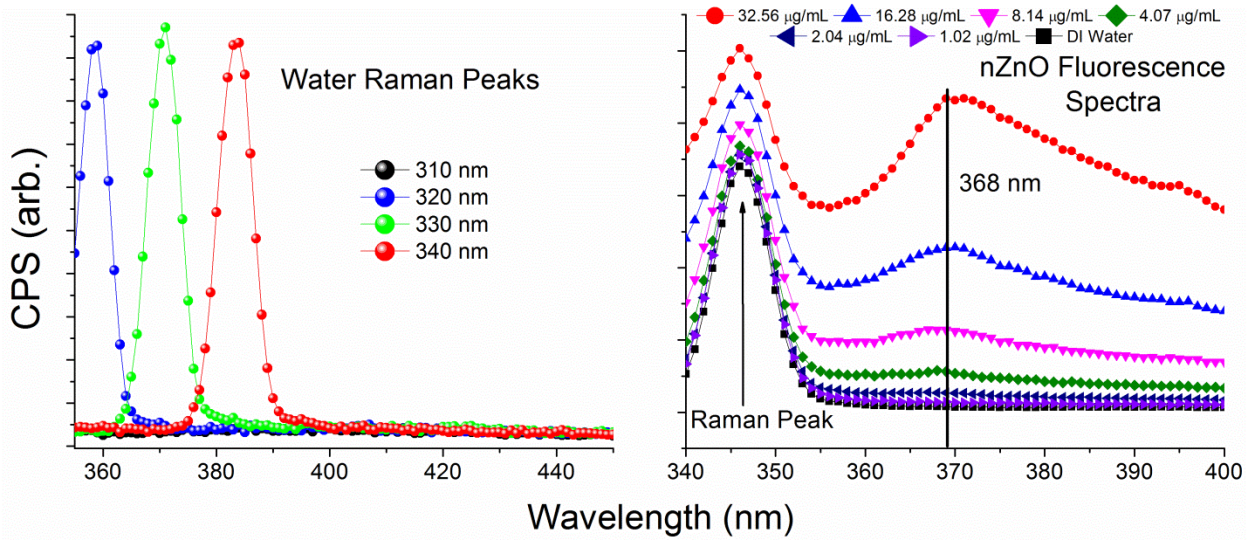


**Figure S1. Spectrofluorometric data from water and nZnO. (left) Raman peaks associated with water appear in the same region as the nZnO fluorescence peak when using a higher wavelength as the excitation source. A 310 nm excitation was chosen to prevent convolution of the nZnO fluorescence peak with the Raman peak. (right) The fluorescence spectra of nZnO at various concentrations using a 310 nm excitation source. The peak intensity at 368 nm was used to monitor nZnO dissolution and convert counts per second (CPS) to concentration.**

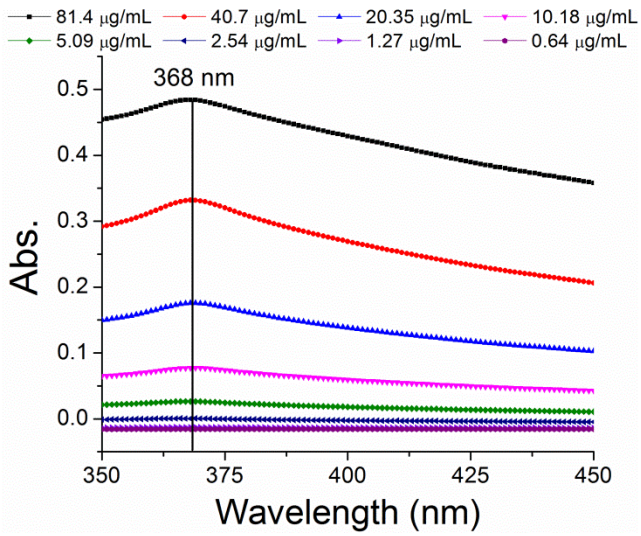


**Figure S2. UV/vis data of nZnO. Example absorbance spectra of nZnO for various concentrations, demonstrating the max absorbance at 368 nm. The peak intensity value at 368 nm was used to convert nZnO absorbance to concentration for dissolution studies.**

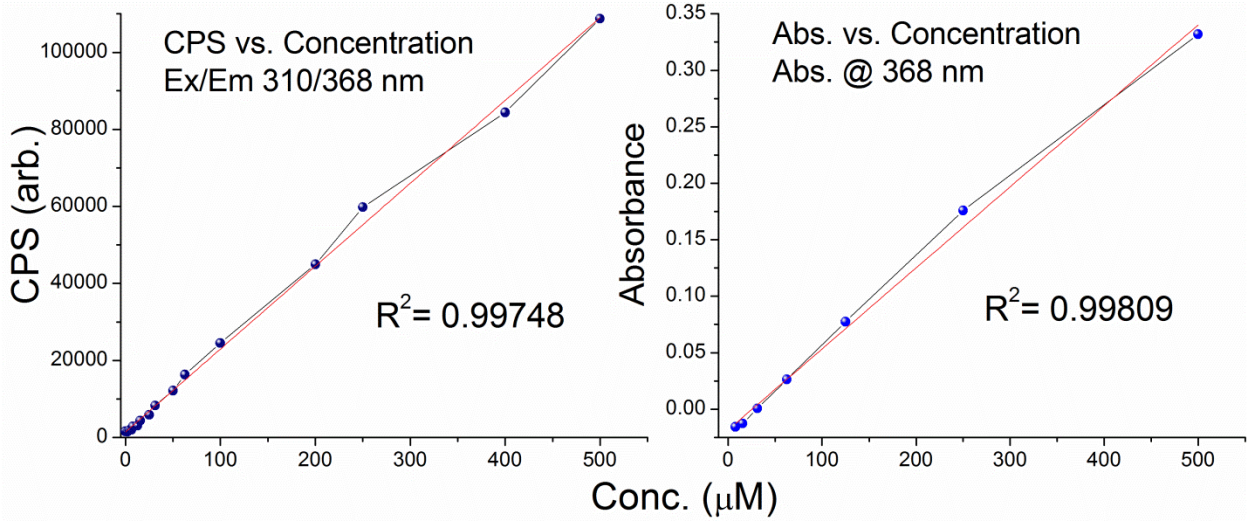


**Figure S3. Plots of fluorescence (left) and absorbance (right) vs. concentration. There is a high linear correlation between nZnO CPS/Abs. and concentration up to 500 μM (40.7 μg/mL), allowing simple conversion for real-time quantitative analysis of nZnO dissolution.**

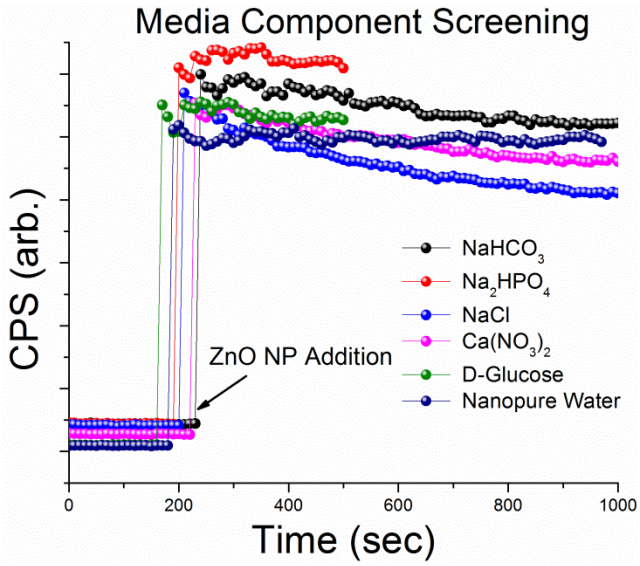


**Figure S4. Screening of multiple media components at biologically relevant concentrations (obtained from ATCC product data sheet for RPMI 1640 medium; product # 30-2001) demonstrate high stability of nZnO (40.7 µg/mL) in various solutions. The slow decrease in CPS for these solutions is likely due to sedimentation of nZnO.**

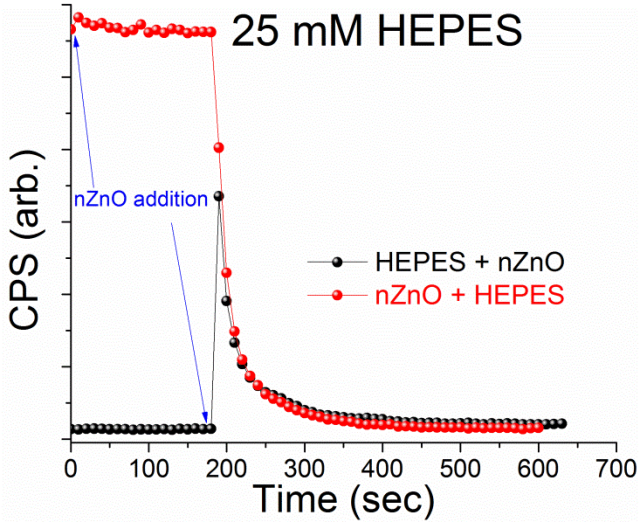


**Figure S5. Rapid dissolution of nZnO (40.7 µg/mL) in 25 mM HEPES buffer. Adding nZnO to the solution already containing HEPES (black) never achieved the CPS expected for the concentration used. Switching the approach (red) by suspending nZnO in solution and then adding the buffer shows the same kinetics profile but retains the information lost during the time of addition. All subsequent experiments suspended nZnO in solution first, then added buffer to retain all dissolution kinetics information.**

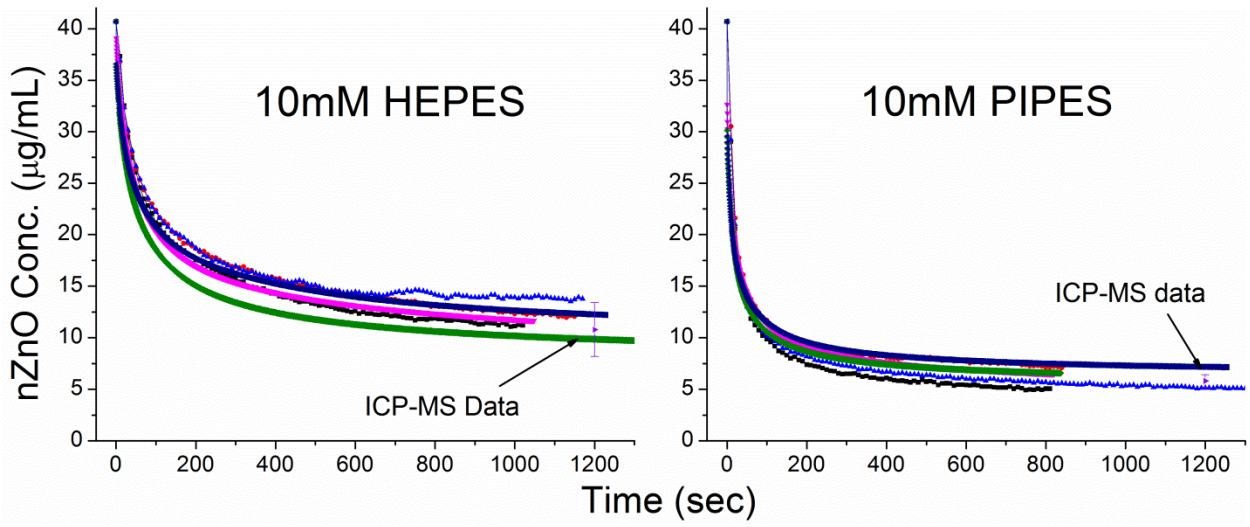


**Figure S6. Two examples of triplicated measurements of nZnO (40.7 µg/mL) in Good's buffers. CPS and Abs. were converted into concentration by using the linear correlation in Figure S3. Triplicate of fluorescence and absorbance measurements are plotted (n=6) for each buffer demonstrating both methods are highly reproducible, consistent, and accurate. ICP-MS was utilized to confirm the accuracy of converting spectra information to concentration.**

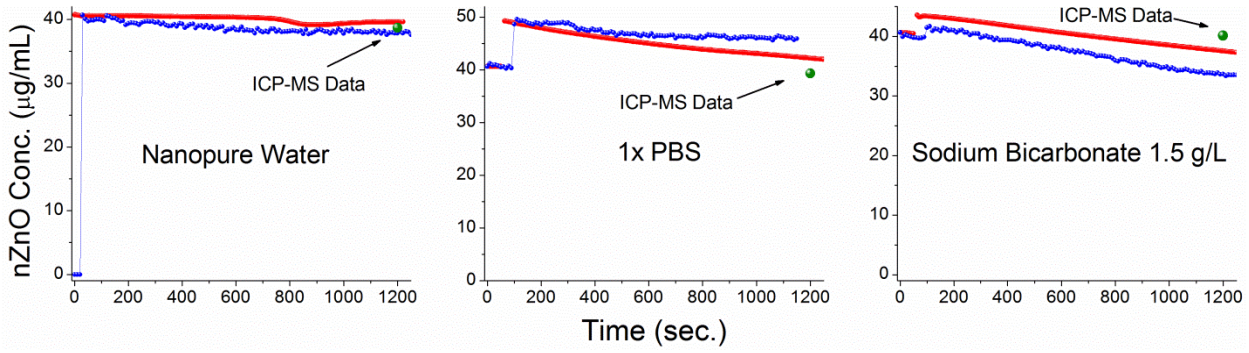


**Figure S7. Additional representative plots of nZnO (40.7 µg/mL) in nanopure water, phosphate buffered saline (PBS) and sodium bicarbonate. nZnO is stable in nanopure water over the 20 minute time course demonstrating kinetics is due to interactions with the media components. Interestingly, in both PBS and sodium bicarbonate, the apparent concentration of nZnO increased upon addition of the buffer. This is likely due to formation of zinc phosphates and zinc carbonates respectively, causing an increase in both absorbance and fluorescence measurements.**

## Characterization

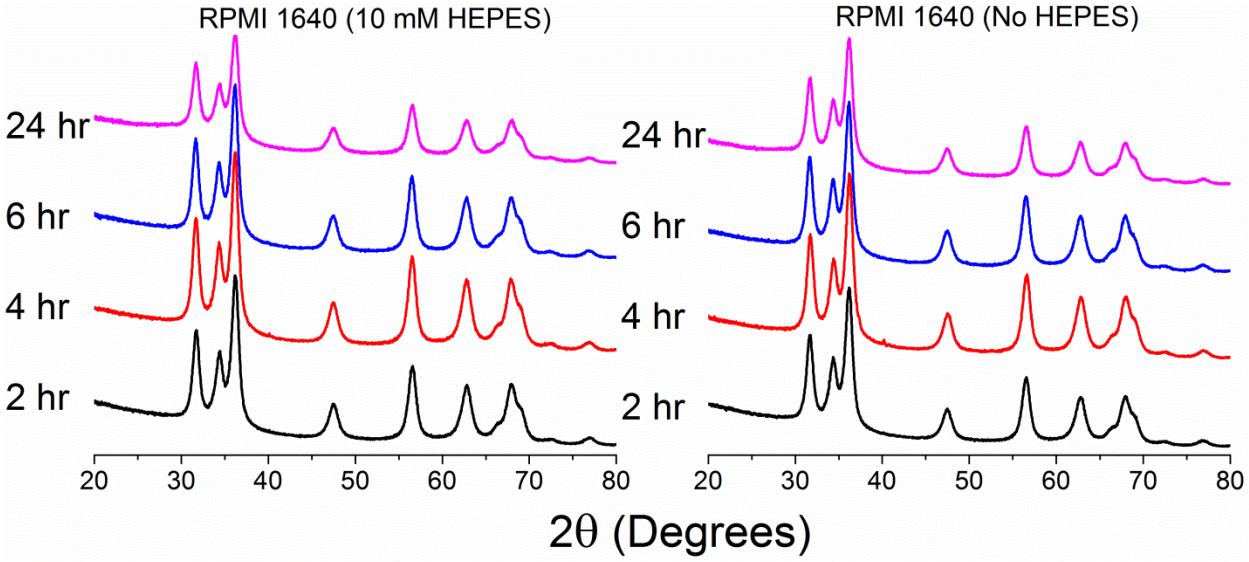


**Figure S8. XRD spectra of nZnO (40.7 µg/mL) post incubation in RPMI 1640 cellular media at various time points. In both conditions (with and without 10 mM HEPES) only the wurzite crystal phase of ZnO was detected over the 24 hour time course. No peaks from zinc phosphate or zinc carbonate were detected, however in both cases the calculated average crystal size reduced from ~9.3 nm to ~7.5 nm.**

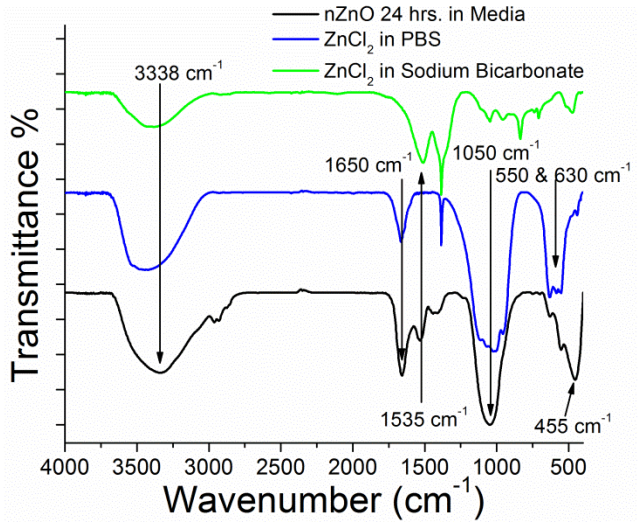


**Figure S9. FTIR spectra of nZnO incubated in RPMI cellular media for 24 hours and precipitate collected from 50mM $ZnCl_2$ solution dispersed in phosphate buffered saline (PBS) or sodium bicarbonate. The Zn-O modes at 455 $cm^{-1}$ are not present in the zinc carbonate/phosphate precipitant. Spectra of the controls confirms peak positions in literature that attribute the 550, 630, and 1050 $cm^{-1}$ peaks to $PO_4^{3-}$ bending/stretching modes, 1650 $cm^{-1}$ to crystalline water and 1535 $cm^{-1}$ to C=O stretching from carbonate.**

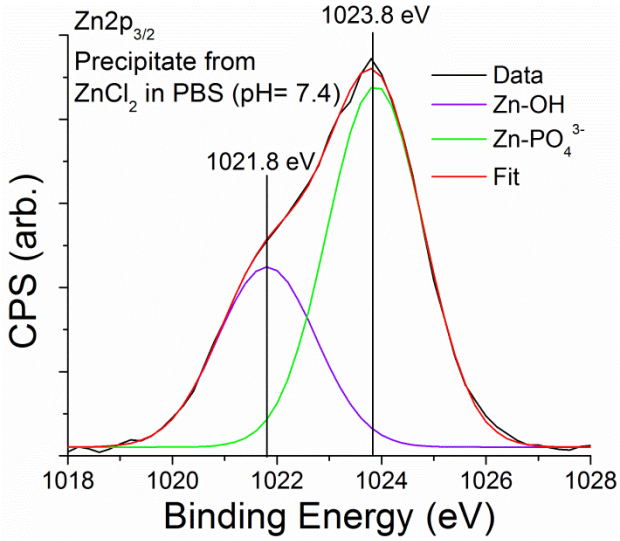


**Figure S10. Core level XPS spectra of the $Zn2p_{3/2}$ region. $ZnCl_2$ solution was dispersed in PBS (pH= 7.4) and the precipitate was collected via centrifugation and subsequently dried for 24 hours. Peak deconvolution demonstrates two zinc species with a chemical shift of ~2.0 eV attributed to Zn- $PO_4^{3-}$ and Zn-OH.**

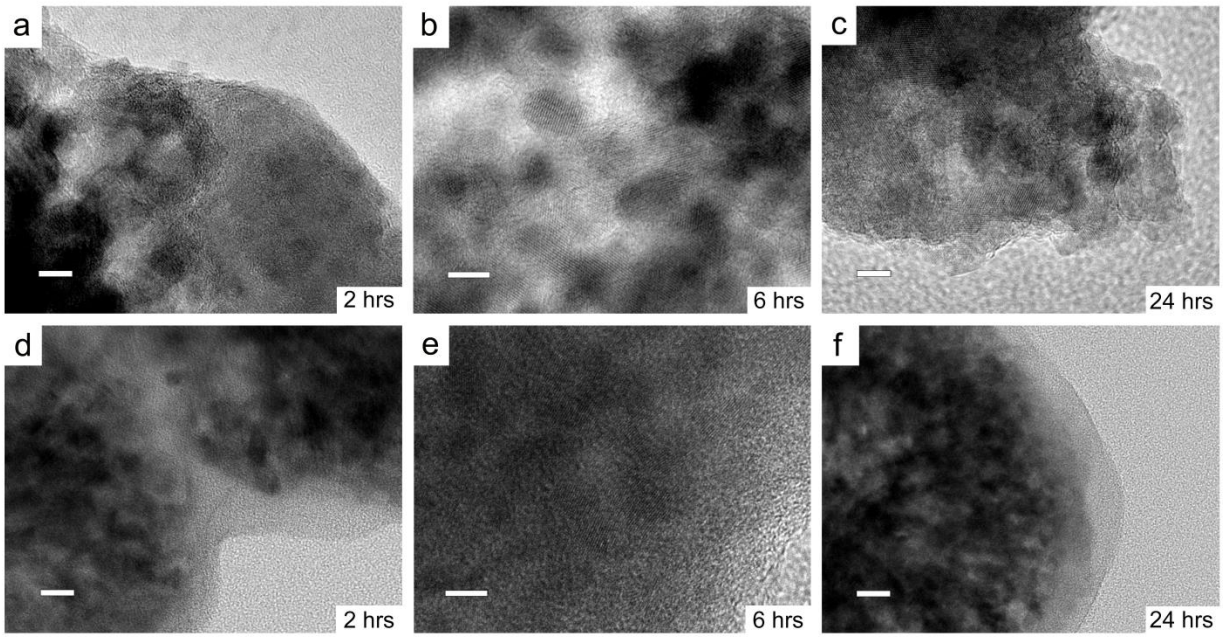


**Figure S11. HRTEM images of nZnO post incubation in RPMI 1640 with (a)-(c) and without 10 mM HEPES (d)-(f). (a)-(c) scale bar: 5 nm; Images show pieces of irregular shaped nZnO aggregates. Porosity of the aggregates increased and the amorphous zinc phosphate/carbonates are spread throughout with individual nZnO crystals embedded. Scale bars: 10 nm (d), 5 nm (e) and 20 nm (f). (d)-(f) nZnO images show the amorphous precipitants forming a matrix on the exterior of the aggregates, binding the particles together. The HRTEM images show the individual nZnO crystals comprising the aggregates are more densely packed than in the media containing HEPES (top row). It appears the slower dissolution rate in HEPES free media causes the precipitants to form on the exterior of the aggregates instead of causing loss of particle integrity, resulting in higher porosity and causing pieces of aggregates to separate from the particle.**

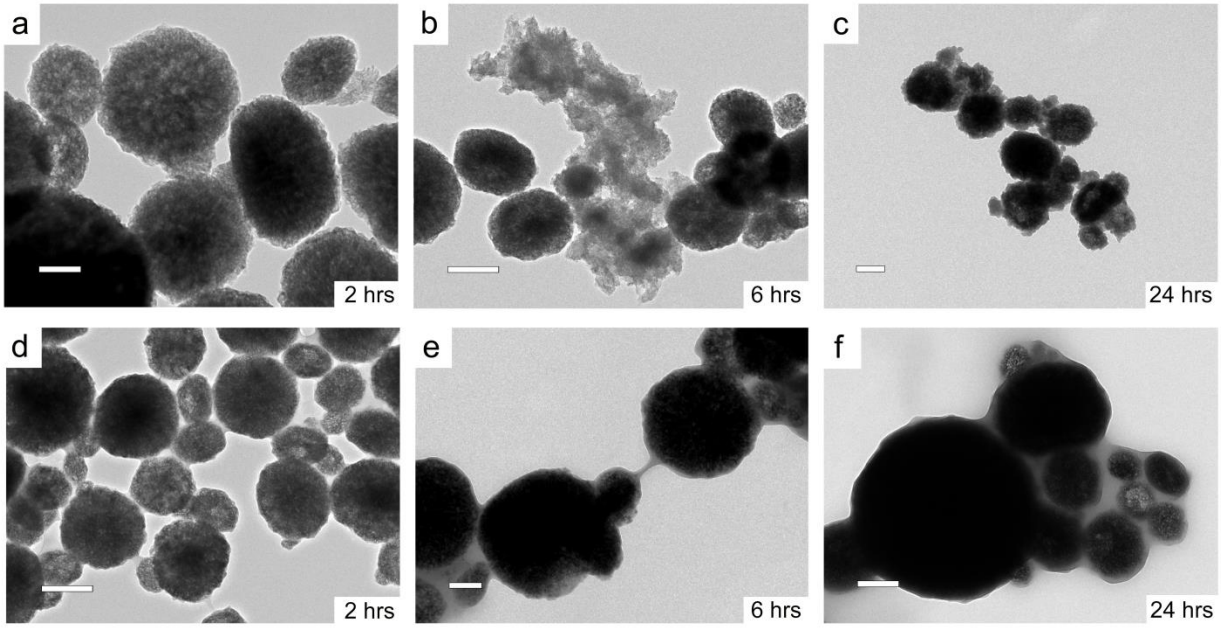


**Figure S12. Scale bars: 200 nm except (a) and (e) (100 nm). Additional images of nZnO incubated in media with (a-c) and without (d-f) 10 mM HEPES at 2, 6 and 24 hours. (a)-(c) Irregular shaped precipitants are seen in media containing HEPES and the spherical shape of the aggregates is lost over the time course. (d)-(f) Matrix formation around the particles is seen when omitting HEPES from the media. Many aggregates are bound together and particles appear to retain their spherical morphology. This would impact the dispersion stability of the nanoparticles and formation of precipitants (top row) may contribute to the overall toxicity profile of nZnO in viability assessments.**

**Time-lapse Video**. (See materials and methods for experimental details) Confocal microscopy time-lapsed video demonstrates the dissolution of nZnO upon the addition of HEPES. The first part of the video shows nZnO in nanopure water as a control to ensure any changes to nZnO wasn't due to dissolution or solubility in water. Upon addition of HEPES, the majority of nZnO disappears from view.